2024 IEEE International Conference on Robotics and Automation (ICRA 2024)
May 13-17, 2024. Yokohama, Japan

Design of a Front-enveloping Powered Exoskeleton Considering Optimal Distribution of Actuating Torques and Center of Mass

Jeongsu Park, Kyeongsu Shi, Gunhee Lee, Hyojun An, Seunghwan Kim, Chanyoung Ko, Taeyeon Kim, Hyeongjun Kim, and Kyoungchul Kong

Abstract— **Traditionally, powered exoskeletons have predominantly featured a back-enveloping design due to its simplicity in both implementation and user donning. However, this design results in a backward shift of the center of mass (CoM) in the sagittal plane. This paper identifies the limitations of existing design approaches and determines the optimal anterior-posterior (A/P) CoM position considering factors like actuating power, balance in the neutral posture, and user's hand workspace. Our optimization analysis recommends placing the CoM in front of the user. We address historical constraints on front-enveloping designs and propose solutions. Furthermore, we validate the usability of our designed exoskeleton through testing with a complete paraplegic user.**

I. INTRODUCTION

In the design of legged robots, careful consideration of the arrangement of components is essential, as the feasible range of motions and balanced postures can undergo sudden changes contingent upon weight distribution dynamics [1]. Specifically, for bipedal walking robots with narrow support bases, convention has dictated positioning the Center of Mass (CoM) at the support polygon's center [2]–[4]. This approach is driven by concerns regarding walking stability and related factors [5].

However, it is worth noting that, despite sharing similarities with bipedal walking robots, all powered exoskeletons developed to date have adhered to a "Back-enveloping" approach, whereby the exoskeleton frame envelops the user from behind [6]–[8]. This design choice results in a significant posterior shift of the CoM. In this posterior portion, which resembles a backpack, components such as batteries and a central control unit are housed. For powered exoskeletons equipped with multiple active degrees of freedom in hip joints, including hip ab/adduction and rotation, these actuators are also typically attached to the rear of the user [9], [10]. Two primary reasons underpin the preference for the back-enveloping design. Firstly, the range of motion (RoM) of the human hip extension is relatively limited (around 30 degrees), whereas hip flexion boasts a significantly broader RoM (approximately 120 degrees). Secondly, during the donning process, powered exoskeletons often require deactivation, followed by the user transferring into a seated position. Consequently, maintaining an unobstructed front for the user becomes imperative.

However, this unique feature of back-enveloping exoskeletons, characterized by the posterior CoM shift, poses challenges for users. It often necessitates forward-leaning postures to prevent backward falls [11]–[13], impacting visibility [14], and causing discomfort [15]–[17]. Users may even require auxiliary support during sit-to-stand motions if the exoskeleton lacks sufficient power due to the longer moment arm between the knee and the upper body's CoM during this movement [18].

To mitigate these issues, optimizing the CoM position during the design phase becomes essential. An alternative worth exploring is the front-enveloping exoskeleton, a design approach introduced in this paper. However, the mechanical structure necessitates high stiffness to accommodate dynamic movements, while bulky batteries and control boards, centrally located to supply power and signals to both legs, contribute to the central volume of the exoskeleton. This central volume limitation, in turn, constrains the user's hand workspace.

This paper presents a method for determining the optimal anterior-posterior CoM position of a powered exoskeleton, taking all these factors into account. Furthermore, we introduce the design methodologies for a front-enveloping powered exoskeleton and the docking motion required for front-side donning. To assess the feasibility and usability of our proposed design, we conduct practical trials with individuals who have complete paraplegia, representing a potential user base.

II. DESIGN OPTIMIZATION: DETERMINING FRONT-BACK WEIGHT DISTRIBUTION

In this section, we determine the optimal front-back weight distribution for a powered exoskeleton. Since the optimal weight distribution varies depending on the objective of the robot, this section also covers the target motions of the powered exoskeleton and the selection of number of active joints required to implement these motions, including the actuating power for each joint.

A. Objective Function Formulation

When designing a powered exoskeleton, it's crucial to engineer the actuators to handle the maximum required power necessary to move both the person and the powered exoskeleton effectively. If the required maximum actuating power changes depending on the weight distribution, it would

*This work was supported by the National Research Foundation of Korea(NRF) grant funded by the Korea government(MSIT)(No.2022R1A3B1077880)

The authors are with the Department of Mechanical Engineering, Korea Advanced Institute of Science and Technology, Daejeon, Republic of Korea, 34141, email: jeongsu.park, shiks, gh003008, gywns99@kaist.ac.kr, shkim512, kkyle0927, ty.kim, khj970311, kckong@kaist.ac.kr

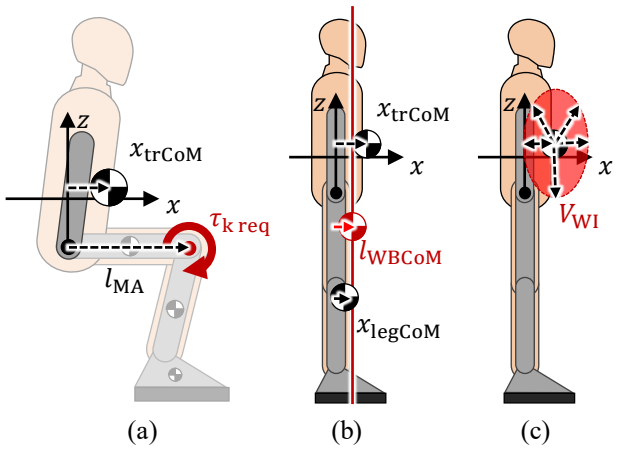

Fig. 1. Objective function explanation. (a) Sit-to-stand knee actuation torque, (b) whole body CoM position and (c) user's hand workspace interrupting volume in the neutral standing posture.

naturally be better to determine the weight distribution in a way that reduces the required actuating power. This not only prevents the weight of the actuator from increasing, but also affects many areas, such as lowering the maximum discharge current of the Battery Management Systems (BMS) or reducing the thickness of the power line of the entire robot. Referring to literature calculating joint torque by forward kinematics from measured human motion data and ground reaction force (GRF) [19], it can be seen that the highest joint torque is used in knee extension during the sit-to-stand (or similar movement, climbing stairs) movements. Since the powered exoskeleton perform movements similar to human, it is reasonable to assume that powered exoskeleton also require the maximum actuating torque on the knee.

The position of the center of mass of the trunk, which can clearly define the posture and has a certain influence on the objective function, is used. It is because although the stance leg posture is limited to a posture similar to the thigh in Fig. 1(a) in the case of the swing leg, the posture of thigh cannot be specified. Based on the situation that requires the maximum actuating force, when the thigh angle is perpendicular to the gravitational acceleration, the knee torque required to lift the upper body is,

$$\tau_{\text{k req}} = m_{\text{tr}}(x_{\text{trCoM}} - l_{\text{MA}})g, \tag{1}$$

where m_{tr} is the mass of the powered exoskeleton's upper body, x_{trCoM} is the horizontal distance from the hip joint to the center of gravity of the upper body, and l_{MA} is the moment arm and is equal to the length of the user's thigh.

The second element of the objective function is how far the overall center of gravity is located from the center of the support polygon in neutral standing posture. The neutral standing posture is the position where most of the time is spent while using the lower limb powered exoskeleton. If the center of gravity locates outside of the support polygon in this posture, it would coerce the user to lean either forward or backward to maintain balance [20]. Maintaining this uncomfortable posture is required not only for the stand still but also during walking to maintain balance [21]. Therefore, the horizontal distance from the CoM of the whole body to the center of support polygon which is same with the center of the foot is denoted as l_{WBCoM} and designated as the second component of the objective function.

$$l_{\text{WBCoM}} = \frac{m_{\text{tr}}x_{\text{trCoM}} + m_{\text{leg}}x_{\text{legCoM}}}{m_{\text{tr}} + m_{\text{leg}}} - l_{\text{MF}}, \tag{2}$$

where $x_{\text{leg CoM}}$ represents the horizontal distance from the hip joint to the CoM of the legs in the neutral posture, m_{leg} is the mass of the powered exoskeleton's legs, and l_{MF} is the horizontal distance from the hip joint to the midfoot.

Lastly, the fact that the front-enveloping powered exoskeleton reduces the user's hand workspace will be included in the objective function. As the structure to support the forward shifted CoM increases the front volume of the powered exoskeleton, the last element of the objective function, workspace interrupting volume, can be formulated as,

$$V_{WI} = \max(a_0 x_{\text{trCoM}}^3, 0). \tag{3}$$

Max function is used because the user's hand workspace is not disturbed if the powered exoskeleton trunk's CoM goes backwards and a_0 is the volume increase coefficient.

The overall objective function is defined as J, and the equation for finding the optimal solution is as follows.

$$\underset{x_{\text{trCoM}}, x_{\text{legCoM}}}{\arg\min} \quad J = a_1\tau_{\text{k req}} + a_2 l_{\text{WBCoM}}^2 + a_3 V_{\text{WI}}, \tag{4}$$

where a_1, a_2, and a_3 are scaling factors needed to combine the terms with different physical scales.

B. Parameter Selection from Exoskeleton Usage

As shown in (1) and (2), the optimal solution of the entire objective function varies depending on the values of m_{tr}, m_{leg}, l_{MA}, and l_{MF}. The weight of the powered exoskeleton is primarily dependent on the weight of the actuator, and the length of the powered exoskeleton is directly related to the body length of the user. Therefore, before proceeding with the optimization of the objective function, it is necessary to set the target user and motion to determine the actuating power, number of actuators, and range of user body size.

To include the complete paraplegics in the user pool, the actuating power of the powered exoskeleton will be set to enable complete paraplegics to maintain their balance, walk and stand up without the use of crutches. To follow this, all degrees of freedom should be active, and a total of 10 actuators will be used. The actuating power is selected to accommodate big size user with 185cm and 90kg. From a paper measuring the power of human joints in various movements such as walking, sitting, and climbing stairs [22], the torque and speed that each actuator must produce is shown in the table below. Also, the expected mass of the motor and drive train is shown in Table 1 assumption of using the Allied Motion's MF Series actuator which has high torque density.

TABLE I

REQUIRED POWER AND ESTIMATED MASS OF ACTUATORS

Active Joint	Torque	Angular Velocity	Estimated Mass
Hip Ab/Ad	250Nm	22PRM	1.2kg
Hip Flexor	200Nm	80RPM	3kg
Knee Flexor	200Nm	80RPM	3kg
Ankle P/D	170Nm	50RPM	1.6kg
Ankle In/Ev	70Nm	8RPM	0.3kg
Battery	140A, 48V	400Wh	4kg

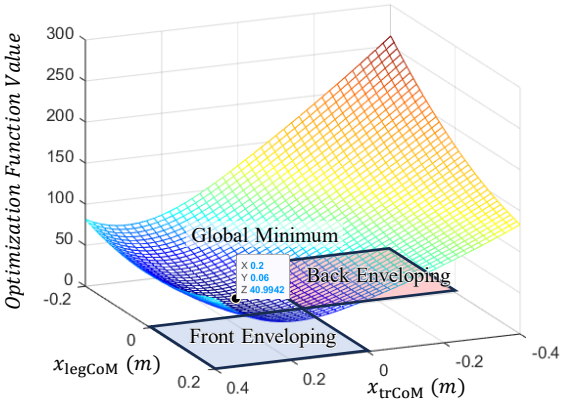

Fig. 2. Optimization result.

The frame is assumed to be an aluminum cloud that surrounds one side of the user's body. Since it does not completely fill the frame, the density is set to 50%. A detailed explanation of the load that the frame must withstand will be provided in Section III. Due to the nature of a bipedal robot, in which stance and swing alternate between left and right, the required actuating torque (current) is periodically focused on one leg. Therefore, the battery must be located in the upper body to allow distribution to the left and right as needed. The central controller is also located in the upper body for real-time control of both legs.

Through Table 1 and the mentioned assumptions, we can set m_{tr} = 16kg, m_{leg} = 38kg, l_{MF} = 0.1m, and l_{MA} = 0.4m. Applying objective function parameters with $a_1 = 1$, $a_2 = 1000$, and a_3 = 1200 which matches the sizes of three components with different units, Fig. 2 show a graphical representation of the objective function and optimization result. It can be concluded that the optimal front-back CoM of each componet should be at $x_{\text{tr CoM}}$ = 0.20m, and $x_{\text{leg CoM}}$ = 0.06m.

III. DESIGN IMPLEMENTATION

In this section, design details of proposed front-enveloping powered exoskeleton will be described. While matching the CoM position as concluded in Section II, we do not forcibly add mass but arrange the components in Table. 1 and aim to make it as light as possible for real application. All the mechanisms such as actuators and frames would be designed to surround the user so that there are no protruding parts of the robot for real application also. In the case of thighs and shanks, a length adjusting mechanism is included to fit the user's body size.

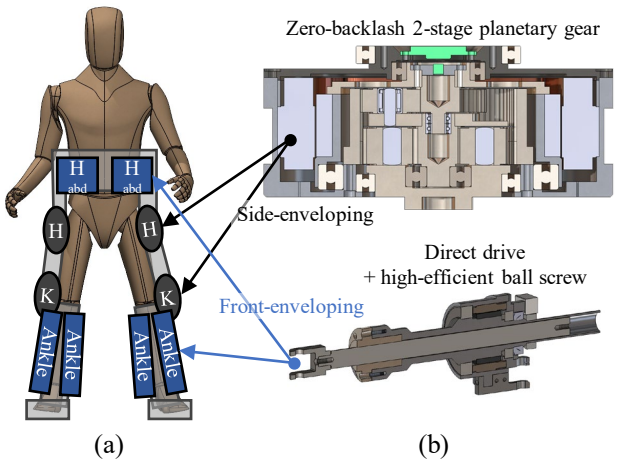

Fig. 3. (a) Overall mass distributing strategy to satisfy the optimized CoM position, (b) customized actuators used in the powered exoskeleton

The primary factors affecting the location of the powered exoskeleton's CoM, listed in order of utmost significance, are 1) the location of the actuator, 2) the location of the frame, and 3) the location of the battery and control board. The actuator should be placed in the front of the user to follow the optimization result. Subsequently, the frame to support the actuator will naturally follow to front. Fig. 3 shows the actuator and frame arrangement strategy to satisfy $x_{\text{tr CoM}}$ and $x_{\text{leg CoM}}$. Detailed explanation would be provided in order of proximity to the trunk.

A. Hip Ab/Adduction Actuation Mechanism

The actuator located at the upper end of the powered exoskeleton is a hip ab/adduction actuator which is placed in front of the person to satisfy x_{trCoM}. In the case of hip ab/adduction, the actuating speed and RoM are very small ($\sim$25 degrees), but the forces that must be withstood, such as the weight of the whole system and the impact force of the ground, are large. In this situation, a slider-crank and ball screw combination was selected as an appropriate actuation mechanism to achieve a high gear ratio around 150 : 1. By connecting directly with a brushless dc motor (MF0076020, Allied Motion, US) and a ball screw (SF1505, THK, Japan), and with several iterations to find the best manufacturing tolerance in the connection parts, high efficiency and low uncertainty of actuator model can be obtained. The stroke of the actuator was determined to be 50mm through kinematic analysis for hip ab/adduction workspace.

B. Hip/Knee Flexion Actuation Mechanism

The hip flexor/extensor and knee flexor/extensor, which are responsible for movement in the sagittal plane, are the joints that require the widest RoM (150 degrees), fastest speed, and large torque in human joint movement. To implement these actuating characteristics, the rotating output of the motor (Allied Motion MF0127020) with a customized 2-stage planetary gear (gear ratio of 24.42) as shown in

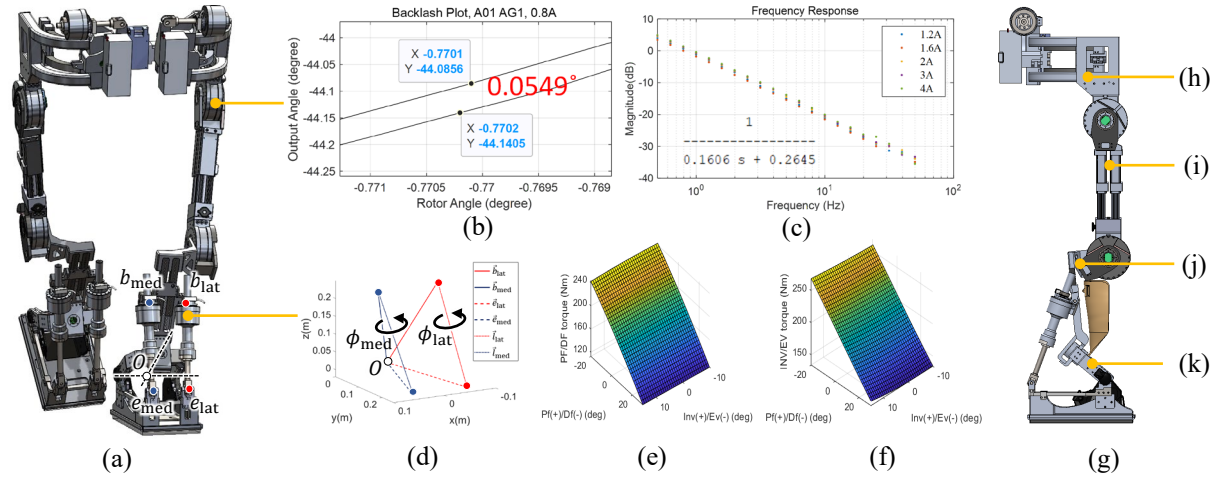

Fig. 4. (a) The whole body of the proposed powered exoskeleton. (b) Backlash measurement and (c) system ID result of the customized zero-backlash high power actuator used in hip and knee flexor. (d) Vector visualization of the parallel actuation mechanism of front-enveloping ankle joint and actuating torque of (e) plantar/dorsi flexion, and (f) inversion/eversion. (g) The whole body of the proposed powered exoskeleton showed in the sagittal plane, and main frames, (h) waist frame, (i) thigh frame, (j) shank frank, (k) ankle and foot frame.

Fig. 3(b) was placed right next to the human joint. As the output power is high, not placing the actuator directly next to the joint would require a strong mechanism for power transmission and unavoidably add a significant amount of weight and volume.

Backlash not only deteriorates the position control performance of the geared actuator, but also lowers the level of practical success in the CoM optimization. Assume the user's leg is 1m, then a 1 degree of backlash in hip and knee actuator generates 2.5cm front-back position gap which is completely uncontrollable. Since a position error at the level of centimeters can alter the results of the optimization randomly during the exoskeleton operation, the backlash should be diminished. To eliminate the backlash, the gear thickness and axis pin thickness were selected through multiple iterations of manufacturing tolerance. The backlash was measured with 18bit high resolution absolute encoder with the conventional backlash measuring test [23]. It can be confirmed that gear sets are finely tuned to have backlash of 0.05 degrees as shown in Fig. 4(b).

The actuators are also designed to conduct the force mode control required for balance control [24]. While it is commonly believed that only 1-stage planetary gear sets can conduct force mode control without force sensors [25], we have reduced the uncertainties in the 2-stage planetary gear sets through highly precise processes. The gears in the reducer are all precisely machined and categorized after measuring with micrometers, ensuring the thickness variance of the planet gears within 0.005mm. As a result, as shown in Fig. 4(c), the current to speed frequency response plot has highly linear model under 70Hz. Although the magnitude of the input changes, it shows the same model.

C. 2-DoF Ankle Actuation Mechanism

As the robot's hip and knee flexion actuators are placed next to the user's joints, the ankle actuation mechanism should be positioned to encircle the front of the user in to fulfill the condition of x_{legCoM}. For the solution, a parallel actuating two linear actuator pair with perpendicular joints from a single center of rotation shown in Fig. 4(a) is devised.

To avoid the complicated computations while controlling parallel mechanism's tricky coupled kinematics which are common problems of them, the base of the linear actuator was design to move like it is on the sphere whose center is orientation O and radius is $|\vec{b}^{\text{idle}}_{\text{med}}|$ as shown in Fig. 4(a). $\vec{b}^{\text{idle}}_{\text{med}}$ is the vector $\vec{b}$ when plantar flexion angle θ_{PF} and inversion angles θ_{Inv} are zero. Then, the angular positions of the linear actuators can be derived from the joint angles, i.e.,

$$R_{\text{PF}} = \begin{bmatrix} 1 & 0 & 0 \\ 0 & \cos\theta_{\text{PF}} & -\sin\theta_{\text{PF}} \\ 0 & \sin\theta_{\text{PF}} & \cos\theta_{\text{PF}} \end{bmatrix},$$

$$R_{\text{Inv}} = \begin{bmatrix} \cos\theta_{\text{Inv}} & -\sin\theta_{\text{Inv}} & 0 \\ \sin\theta_{\text{Inv}} & \cos\theta_{\text{Inv}} & 0 \\ 0 & 0 & 1 \end{bmatrix}, \tag{5}$$

$$\vec{b}_{\text{med}} = R_{\text{PF}} R_{\text{Inv}} \cdot \vec{b}^{\text{idle}}_{\text{med}}, \tag{6}$$

and

$$l_{\text{med}} = |\vec{e}_{\text{med}} - \vec{b}_{\text{med}}|, \text{and} \;\; \dot{\phi}_{\text{med}} = \dot{l}_{\text{med}}/p, \tag{7}$$

where R is rotational matrix, $\vec{b}_{\text{med}}$ is the vector starting from O and heads to the medial actuator base, $\vec{e}_{\text{med}}$ is the vector starting from O and heads to the end effector of the medial actuator, l_{med} is length of the linear actuator, $\dot{\phi}_{\text{med}}$ is angular velocity of medial actuator's motor, and p is the pitch of the ball screw. The vectors are also visualized on the Fig. 4(d). The lateral actuator's position can also be controlled in the same scheme with (5), (6), and (7).

Compared to the mechanism that serially connects the two actuators, both actuators of this parallel mechanism can exert force together in requisite axis, i.e.,

$$\tau_{\text{PF}} = \tau_{\text{med,PF}} + \tau_{\text{lat,PF}},$$

$$\tau_{\text{Inv}} = \tau_{\text{med,Inv}} + \tau_{\text{lat,Inv}}, \tag{8}$$

$$\tau_{i,\hat{n}} = d_{i,\hat{n}} \cdot f_i,$$

and

$$d_{i,\hat{n}} = \frac{|proj_{\hat{n}}\vec{l}_i \times proj_{\hat{n}}\vec{e}_i|}{|proj_{\hat{n}}\vec{l}_i|}. \quad (9)$$

Here, f_i stands for the thrust force of the linear actuator i. From the kinematics solved in the above equations, moment arms can be derived and actuating torque of each axis depending on the θ_{PF}, and θ_{Inv} is shown in Figs. 4(e) and (f). The linear actuators in the proposed parallel mechanism consist of ball screw (SFH1510, THK, Japan) directly connected to the brushless dc motor (MF0060020, Allied Motion, US) without gears. Combination of direct drive and ball screw allows not only position mode control but also force mode controls since it can be assumed as having quasi-zero uncertainties.

D. Frame Design with Dual Support Structure

During walking, a human body receives ground reaction forces approximately 1.5 times the body weight with each heel strike [26]. Accordingly, all frames of the proposed powered exoskeleton have been designed to have a safety factor of 3 or higher when subjected to a 2000N load. Furthermore, to ensure that the end of a leg, which can be as long as 1 meter, does not inadvertently step into unintended places due to elastic deformation, the primary areas subjected to loads causing end effector deformation are designed to have a dual support structure.

The waist frame as shown in Fig. 4(h), which wraps around the front of the uppermost part of a user's waist, is composed with two evenly spaced bent pipes. This structure provides robustness against moments in the coronal plane generated by ground impact, with respect to the abductor axis. The thigh frame of the powered exoskeleton allows the wearer to adjust the distance between the hip actuator and knee actuator by turning a handle directly. The thigh frame, including the linkage connecting to both the hip actuator and knee actuator, is designed with a dual structure as shown in the Fig. 4(i), providing structural robustness not only against tensile/compressive loads but also against bending and torsional loads from various directions.

To support the two ankle linear actuators located in front of the user's shank, the shank frame shown in Fig. 4(j) extends forward in front of the user. To prevent stress concentration in the connecting section between the thigh frame and the shank which have to be bend 90 degrees, it bends in three segments. In addition, it is designed with a wide truss structure to withstand moments in the sagittal and coronal planes simultaneously while remaining lightweight. The length adjustment part of the shank frame efficiently supports moments in the coronal plane using two evenly spaced bars. As shown in Fig. 4(k), below the shank frame, ankle joints are composed of two pairs of plates. The foot connected to the plantar/flexion joint is supporting two linear actuator pairs through stainless steel angle brackets and an aluminum frame, ensuring sufficient rigidity. The sole of the foot is also made of lightweight aluminum plates, but two plates are used with a spacing to provide sufficient rigidity against bending moments. Load cells are attached between the two aluminum plates to obtain GRF information.

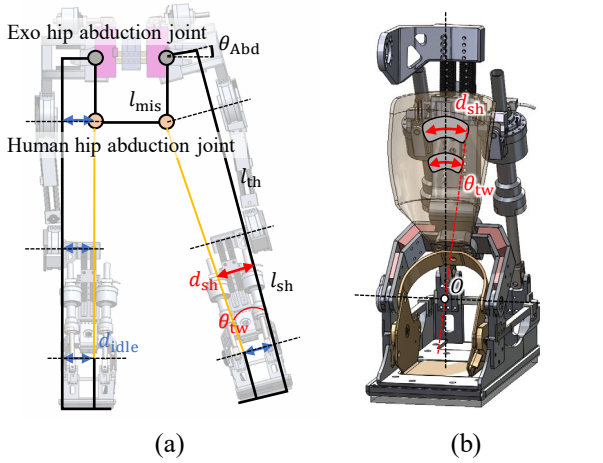

Fig. 5. (a) Problems arising from hip abduction joint misalignment and (b) shank suit design to address them.

E. Dealing with Hip Flexion RoM and Hip Abductor Misalignment

When looking at the completed robot in Figs. 4(a) and (g), it can be observed that the hip abductor joint is positioned higher than the hip flexor joint. The design secures the hip flexion RoM which is the design challenges of front-enveloping as mentioned. The human-exoskeleton attaching part (referred as the "suit" here after) and frame should be designed to eliminate the adverse effects caused by misalignment between the powered exoskeleton and the user.

The shank suit must securely grip the human shank in a face-to-face manner under any circumstances [27]. However, in situations where exoskeleton and user's hip joint has misalignment of l_{mis}, as shown in Fig. 5(a), misalignment can cause angular twist and lateral distance changes between the powered exoskeleton and the user's shank. The twist angle and distance changes can be calculated as,

$$\theta_{\mathrm{tw}} = \arctan\left(\frac{l_{\mathrm{mis}} \sin\theta_{\mathrm{Abd}}}{l_{\mathrm{th}} + l_{\mathrm{sh}}}\right), \quad (10)$$

and

$$d_{\mathrm{sh}} - d_{\mathrm{idle}} = a_4 l_{\mathrm{sh}} \tan\theta_{\mathrm{tw}}, \quad (11)$$

where θ_{Abd} is the hip abduction angle of the powered exoskeleton, l_{th} and l_{sh} is the length of the user's thigh and shank. d_{sh} and d_{idle} is the distance from the exoskeleton to the suit fixed parts of the user on the shank when misaligment happens and not, respectively. a_4 is the scaling value that can decide the fixed parts height on the shank.

Fig. 5(b) presents the mechanism to address this issue. The misalignments can be corrected by using rotation and slider joints at the shank suit while the foot suit is firmly fixed to the powered exoskeleton. The suit follows exoskeleton's movements well in the sagittal plane, covering all misalignments in the lateral direction with a face-sliding structure.

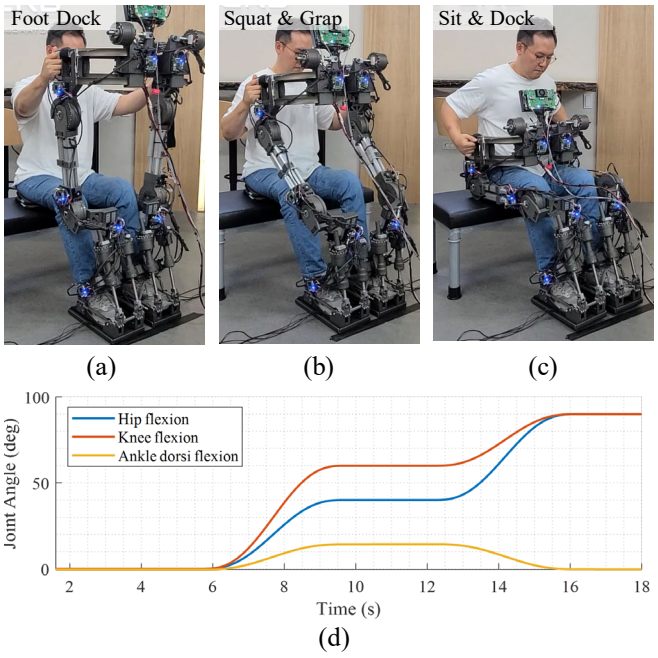

Fig. 6. (a), (b), (c) Demonstration of donning the powered exoskeleton, and (d) joint trajectory of the donning motions.

Applying maximum θ_{Abd} of 15 degrees and scaling value a_4 = 0.7 in (10) and (11), the cover range of angular twist and lateral distance should be designed to 4 degrees, and 60mm for the largest effect of misalignment in a small size user.

F. Design of Front Donning Motion

The rear part of the exoskeleton has been designed entirely hollow. Users can enter the exoskeleton through this empty space. Unlike traditional powered exoskeletons, the user transfers onto the sitted robot, the proposed front-enveloping powered exoskeleton, conversely, allows users to sit comfortably while the exoskeleton docks over them.

The whole donning scenario is illustrated in Fig. 6. In Fig. 6(a), the user is seated on an empty chair. As the powered exoskeleton approaches to the front of the user, the user uses one hand to hold the thigh and the other hand to hold the shank, adjusting and placing the foot onto the powered exoskeleton's foot. Subsequently, in Fig. 6(b), the powered exoskeleton performs a squatting posture, lowering the waist as much as possible, and the user grips the handles attached to the powered exoskeleton. Finally, as shown in Fig. 6(c), the powered exoskeleton is pulled toward the user's body.

During the donning motion, powered exoskeleton's CoM should strictly located on it's support polygon for user's safety in the case of power failure and also to reduce the user's load. Generated hip, knee ankle trajectory on the sagittal plane is shown in Fig. 6(d).

IV. PERFORMANCE EVALUATION

The proposed design, as depicted in Fig. 7, has been successfully manufactured. The measured mass of the torso (m_{tr}) and legs (m_{leg}) after fabrication is 15.26 kg and 39.13 kg,

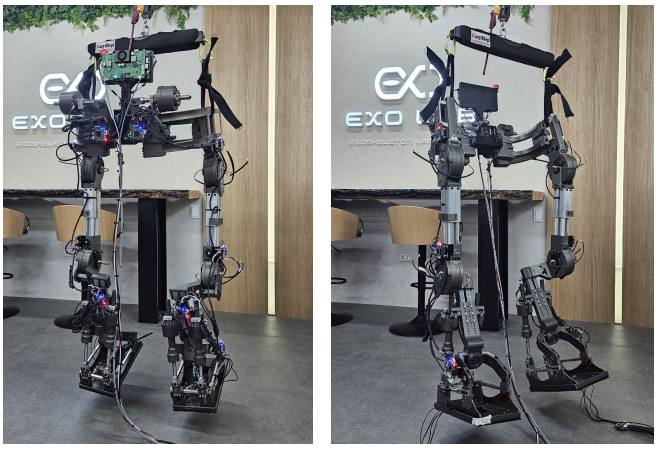

Fig. 7. Prototype of the proposed exoskeleton design.

respectively. In the CAD file (Solidworks, Dassault, France), the calculated values for x_{trCoM} and x_{legCoM} are 0.198 m and 0.057 m, respectively, which exhibit only millimeter-level discrepancies from the optimization results. The most prominent protrusion in the proposed front-enveloping powered exoskeleton is the hip ab/adduction actuator, extending 108 mm from the user's foremost point, the belly. This ensures free hand movements of the user so that the user can hold big stuffs such as boxes while using the exoskeleton as presented in the complemental video. The system is controlled using main control units comprising an STM microprocessor, custom-designed power board, and motor drivers. We successfully demonstrated the front-donning motion, as shown in Figs. 6(a)-(c). The participant involved in the demonstration has a T10 spinal cord injury (SCI) and has a body size of 183 cm and weight of 90 kg. Thanks to the proposed innovative back hollow design and the docking motion, even individuals with disabilities can independently don the powered exoskeleton, eliminating the need for external assistance.

V. CONCLUSIONS

We introduce a novel design method for a lower limb powered exoskeleton that optimizes the Center of Mass (CoM) position for various operational scenarios. This approach has led to the development of a pioneering front-enveloping powered exoskeleton. Moreover, we have successfully demonstrated the donning of this exoskeleton by users with complete paraplegia. With its robust stiffness and substantial actuating power, this powered exoskeleton holds the potential to enable individuals with complete paraplegia to walk in real outdoor environments.

Looking ahead, our future work will focus on one of the distinctive features of our proposed exoskeleton: "self-donning for complete paraplegics". We will also delve into control algorithms and motion generation strategies for the exoskeleton in our upcoming studies, with the ultimate goal of showcasing the independent mobility of individuals with walking disabilities.

REFERENCES

[1] S. Seok, A. Wang, M. Y. Chuah, D. J. Hyun, J. Lee, D. M. Otten, J. H. Lang, and S. Kim, "Design principles for energy-efficient legged locomotion and implementation on the mit cheetah robot," *IEEE/ASME Transactions on Mechatronics*, vol. 20, no. 3, pp. 1117–1129, 2015.

[2] H. Jeong, O. Sim, H. Bae, K. Lee, J. Oh, and J.-H. Oh, "Biped walking stabilization based on foot placement control using capture point feedback," in *2017 IEEE/RSJ International Conference on Intelligent Robots and Systems (IROS)*, pp. 5263–5269, 2017.

[3] H.-M. Joe and J.-H. Oh, "Balance recovery through model predictive control based on capture point dynamics for biped walking robot," *Robotics and Autonomous Systems*, vol. 105, pp. 1–10, 2018.

[4] N. Van der Noot and A. Barrea, "Zero-moment point on a bipedal robot under bio-inspired walking control," in *MELECON 2014-2014 17th IEEE Mediterranean Electrotechnical Conference*, pp. 85–90, IEEE, 2014.

[5] J. Englsberger, C. Ott, and A. Albu-Schäffer, "Three-dimensional bipedal walking control based on divergent component of motion," *IEEE Transactions on Robotics*, vol. 31, no. 2, pp. 355–368, 2015.

[6] A. Zoss, H. Kazerooni, and A. Chu, "Biomechanical design of the berkeley lower extremity exoskeleton (bleex)," *IEEE/ASME Transactions on Mechatronics*, vol. 11, no. 2, pp. 128–138, 2006.

[7] A. J. Young and D. P. Ferris, "State of the art and future directions for lower limb robotic exoskeletons," *IEEE Transactions on Neural Systems and Rehabilitation Engineering*, vol. 25, no. 2, pp. 171–182, 2017.

[8] H. Lee, P. W. Ferguson, and J. Rosen, "Chapter 11 - lower limb exoskeleton systems—overview," in *Wearable Robotics* (J. Rosen and P. W. Ferguson, eds.), pp. 207–229, Academic Press, 2020.

[9] T. Zhang, M. Tran, and H. Huang, "Design and experimental verification of hip exoskeleton with balance capacities for walking assistance," *IEEE/ASME Transactions on Mechatronics*, vol. 23, no. 1, pp. 274–285, 2018.

[10] C. Meijneke, G. van Oort, V. Sluiter, E. van Asseldonk, N. L. Tagliamonte, F. Tamburella, I. Pisotta, M. Masciullo, M. Arquilla, M. Molinari, A. R. Wu, F. Dzeladini, A. J. Ijspeert, and H. van der Kooij, "Symbitron exoskeleton: Design, control, and evaluation of a modular exoskeleton for incomplete and complete spinal cord injured individuals," *IEEE Transactions on Neural Systems and Rehabilitation Engineering*, vol. 29, pp. 330–339, 2021.

[11] A. Yang, P. Asselin, S. Knezevic, S. Kornfeld, and A. Spungen, "Assessment of in-hospital walking velocity and level of assistance in a powered exoskeleton in persons with spinal cord injury," *Topics in spinal cord injury rehabilitation*, vol. 21, no. 2, pp. 100–109, 2015.

[12] K. W. Park, J. Park, J. Choi, and K. Kong, "Adaptive gait pattern generation of a powered exoskeleton by iterative learning of human behavior," in *2020 IEEE/RSJ International Conference on Intelligent Robots and Systems (IROS)*, pp. 3410–3415, 2020.

[13] J. Choi, B. Na, P.-G. Jung, D.-w. Rha, and K. Kong, "Joint trajectory generation and motion control of a wearable robot for complete paraplegics based on forward inflection walking," in *2017 IEEE Conference on Control Technology and Applications (CCTA)*, pp. 1277–1281, 2017.

[14] H. Choi, B. Na, J. Lee, and K. Kong, "A user interface system with see-through display for walkon suit: a powered exoskeleton for complete paraplegics," *Applied Sciences*, vol. 8, no. 11, p. 2287, 2018.

[15] A. J. Smith, B. N. Fournier, J. Nantel, and E. D. Lemaire, "Estimating upper extremity joint loads of persons with spinal cord injury walking with a lower extremity powered exoskeleton and forearm crutches," *Journal of Biomechanics*, vol. 107, p. 109835, 2020.

[16] J. Park, D. Lee, K.-W. Park, and K. Kong, "Reduction of ground impact of a powered exoskeleton by shock absorption mechanism on the shank," in *2021 IEEE International Conference on Robotics and Automation (ICRA)*, pp. 2085–2090, 2021.

[17] J. Park, D. Lee, and K. Kong, "Shank shock absorption mechanism and associated gait pattern design for reduction of ground impact of a powered exoskeleton," *International Journal of Control, Automation and Systems*, vol. 21, pp. 1959–1969, Jun 2023.

[18] J. Choi, K.-W. Park, J. Park, and K. Kong, "The history and future of the walkon suit: A powered exoskeleton for people with disabilities," *IEEE Industrial Electronics Magazine*, pp. 2–15, 2021.

[19] J.-C. Kim, K.-S. Kim, and S. Kim, "Wearable sensor system including optical 3-axis grf sensor for joint torque estimation in real-time gait analysis," in *2014 IEEE/ASME International Conference on Advanced Intelligent Mechatronics*, pp. 112–117, IEEE, 2014.

[20] M.-y. Deng, Z.-y. Ma, Y.-n. Wang, H.-s. Wang, Y.-b. Zhao, Q.-x. Wei, W. Yang, and C.-j. Yang, "Fall preventive gait trajectory planning of a lower limb rehabilitation exoskeleton based on capture point theory," *Frontiers of Information Technology & Electronic Engineering*, vol. 20, pp. 1322–1330, 2019.

[21] G. Sung, K. Kong, and J. Choi, "What is the proper gait pattern for people with paraplegia who wear powered exoskeletons?: Re-examining gait patterns of existing powered exoskeletons," *IEEE Robotics & Automation Magazine*, pp. 2–15, 2023.

[22] K. Serbest, M. Cilli, and O. Eldogan, "Biomechanical effects of daily physical activities on the lower limb," *Acta Orthopaedica et Traumatologica Turcica*, vol. 49, no. 1, pp. 85–90, 2015.

[23] D. E. Whitney, C. A. Lozinski, and J. M. Rourke, "Industrial Robot Forward Calibration Method and Results," *Journal of Dynamic Systems, Measurement, and Control*, vol. 108, pp. 1–8, 03 1986.

[24] C. Ott, M. A. Roa, and G. Hirzinger, "Posture and balance control for biped robots based on contact force optimization," in *2011 11th IEEE-RAS International Conference on Humanoid Robots*, pp. 26–33, 2011.

[25] P. M. Wensing, A. Wang, S. Seok, D. Otten, J. Lang, and S. Kim, "Proprioceptive actuator design in the mit cheetah: Impact mitigation and high-bandwidth physical interaction for dynamic legged robots," *IEEE Transactions on Robotics*, vol. 33, no. 3, pp. 509–522, 2017.

[26] J. Collins and M. Whittle, "Impulsive forces during walking and their clinical implications," *Clinical Biomechanics*, vol. 4, no. 3, pp. 179–187, 1989.

[27] S. V. Sarkisian, M. K. Ishmael, G. R. Hunt, and T. Lenzi, "Design, development, and validation of a self-aligning mechanism for high-torque powered knee exoskeletons," *IEEE Transactions on Medical Robotics and Bionics*, vol. 2, no. 2, pp. 248–259, 2020.